

Kinetics of NH₃-oxidation, NO-turnover, N₂O-production and electron flow during oxygen depletion in model bacterial and archaeal ammonia oxidisers

Linda Hink¹, Pawel Lycus², Cécile Gubry-Rangin¹, Åsa Frostegård², Graeme W. Nicol³,
James I. Prosser¹, Lars R. Bakken²

¹ School of Biological Sciences, University of Aberdeen, Cruickshank Building,
Aberdeen, AB24 3UU, UK

² Faculty of Chemistry, Biotechnology and Food Science, Norwegian University of
Life Sciences, 1432, Ås, Norway

³ Laboratoire Ampère, École Centrale de Lyon, Université de Lyon, 69134, Ecully
CEDEX, France

This article has been accepted for publication and undergone full peer review but has not been through the copyediting, typesetting, pagination and proofreading process which may lead to differences between this version and the Version of Record. Please cite this article as an 'Accepted Article', doi: 10.1111/1462-2920.13914

This article is protected by copyright. All rights reserved.

Originality-Significance Statement

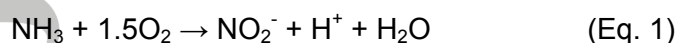
The authors confirm that all of the work is original. Ammonia oxidizing bacteria (AOB) and archaea (AOA) contribute to the emission of the greenhouse gas N_2O . Our study corroborate current understanding of the metabolic pathways leading to higher N_2O production by AOB than by AOA, but provides candid assessments of their possible contribution to N_2O emissions through high resolution gas kinetics and product stoichiometry measured under physiologically realistic and ecologically relevant conditions; low cell density and gradual depletion of oxygen. The data also shed new light on the physiological role of the denitrification pathway in AOB; indicating that it plays a negligible role in sustaining their respiratory metabolism; accounting for less than 1.2% of the electron flow even under severe oxygen limitation. A more plausible physiological role for denitrification is redox balancing, which would explain the high N_2O production rates at 4 mM TAN than at 1 mM. An important environmental implication is that the N_2O yield of AOB increases with increasing ammonium concentration, and that fertilizer application level controls the N_2O/NO_2^- product ratio of nitrification in agricultural soils.

Summary

Ammonia oxidising bacteria (AOB) are thought to emit more nitrous oxide (N_2O) than ammonia oxidising archaea (AOA), due to their higher N_2O yield under oxic conditions and denitrification in response to oxygen (O_2) limitation. We determined the kinetics of growth and turnover of nitric oxide (NO) and N_2O at low cell densities of *Nitrosomonas europaea* (AOB) and *Nitrosopumilus maritimus* (AOA) during gradual depletion of TAN ($\text{NH}_3 + \text{NH}_4^+$) and O_2 . Half-saturation constants for O_2 and TAN were similar to those determined by others, except for the half-saturation constant for ammonium in *N. maritimus* (0.2 mM), which is orders of magnitudes higher than previously reported. For both strains, cell-specific rates of NO turnover and N_2O production reached maxima near O_2 half-saturation constant concentration (2-10 μM O_2) and decreased to zero in response to complete O_2 -depletion. Modelling of the electron flow in *N. europaea* demonstrated low electron flow to denitrification ($\leq 1.2\%$ of the total electron flow), even at sub-micromolar O_2 concentrations. The results corroborate current understanding of the role of NO in the metabolism of AOA and suggest that denitrification is inconsequential for the energy metabolism of AOB, but possibly important as a route for dissipation of electrons at high ammonium concentration.

Introduction

Emissions of nitric oxide (NO) and nitrous oxide (N₂O) from soil and marine environments are mainly driven by heterotrophic denitrification and aerobic ammonia oxidation (e.g. Hu *et al.*, 2015; Santoro *et al.*, 2011; Hink *et al.*, 2016). The pathways leading to N₂O and NO emissions from ammonia (NH₃) oxidising organisms are only partially understood and differ between ammonia oxidising bacteria (AOB) and archaea (AOA). Both groups oxidise ammonia to hydroxylamine by ammonia monooxygenase (Prosser, 1989; Vajrala *et al.*, 2013), which is further oxidised to nitrite (NO₂⁻) by hydroxylamine dehydrogenase (EC 1.7.2.6; formerly known as hydroxylamine oxidoreductase) in AOB (Hooper *et al.*, 1978). Hydroxylamine dehydrogenase has not been identified in AOA, where hydroxylamine oxidation is proposed to involve NO as an essential intermediate. NO is thought to support oxidation of hydroxylamine to two molecules of NO₂⁻, one of which is reduced to NO, mediated by nitrite reductase (encoded by *nirK*; Kozłowski *et al.*, 2016a). NO has been speculated to be an enzyme-bound intermediate in AOB (Arp and Stein, 2003; Bock and Wagner, 2006). However, the reaction stoichiometry is identical in both groups (Eq. 1).



While both groups possess a nitrite reductase, most AOB also possess a gene encoding a nitric oxide reductase, thus enabling them to sustain respiratory metabolism under oxygen (O₂) limitation, using NO₂⁻ and NO as alternative electron acceptors, performing so-called nitrifier denitrification (Arp and Stein, 2003; Stein, 2011). Genes encoding a nitrous oxide reductase have not been identified in the genomes of any cultured ammonia oxidiser, which is consistent with physiological observations (e.g. Chain *et al.*, 2003; Norton *et al.*, 2008; Walker *et al.*, 2010; Campbell *et al.*, 2011; Tourna *et al.*, 2011; Spang *et al.*, 2012). Thus, nitrifier denitrification (by AOB) is hypothetically a strong contributor to N₂O emission from soils, for which there is some circumstantial evidence (Wrage *et al.*, 2001, Kool *et al.*, 2011; Zhu *et al.*, 2013).

During unrestricted aerobic growth, AOB emit a relatively low fraction of the oxidised $\text{NH}_3\text{-N}$ as $\text{N}_2\text{O-N}$ (N_2O yield: $\text{N}_2\text{O-N}$ per $\text{NO}_2^- \text{-N}$ generated from $\text{NH}_3\text{-N}$ oxidised), ranging from ~0.1% in *Nitrosospira* strains (Jiang and Bakken, 1999; Aakra *et al.*, 2001) to ~1% in the type strains *Nitrosospira multiformis* ATCC 25196 and *N. europaea* ATCC 19718 (Jiang and Bakken, 1999; Anderson *et al.*, 1993). Anderson *et al.* (1993) also reported that 2.6% of $\text{NH}_3\text{-N}$ oxidised is emitted as NO by *N. europaea*. N_2O production under fully oxic conditions may result from nitrosation reactions involving both hydroxylamine and NO_2^- (Zhu-Barker *et al.*, 2015) or incomplete oxidation of hydroxylamine by hydroxylamine dehydrogenase resulting in the production of some NO in addition to the main product NO_2^- (Hooper and Terry, 1979; Hooper *et al.*, 1997). Nitrifier denitrification by AOB invariably increases in response to O_2 limitation (Goreau *et al.*, 1980; Remede and Conrad, 1990; Anderson *et al.* 1993; Dundee and Hopkins, 2001; Wrage *et al.*, 2001; Zhu *et al.*, 2013; Stieglmeier *et al.*, 2014), most likely through activation of denitrification enzymes whose expression is not completely repressed by oxygen (Whittaker *et al.*, 2000; Yu and Chandran, 2010), the rate possibly being controlled by competition for electrons between denitrification enzymes and terminal oxidases (Anderson *et al.* 1993). AOA produce N_2O during unrestricted aerobic growth through so-called 'hybrid formation', which is assumed to result from a chemical nitrosation reaction involving the ammonia oxidation intermediates hydroxylamine and NO (Stieglmeier *et al.*, 2014; Kozlowski *et al.*, 2016a). N_2O yield appears to be in the lower range of that for AOB; i.e. 0.004 – 0.23% (Jung *et al.*, 2011; Santoro *et al.*, 2011; Kim *et al.*, 2012; Jung *et al.*, 2014; Stieglmeier *et al.*, 2014) with no or only marginal increase observed under O_2 limitation (Jung *et al.*, 2011; Löscher *et al.*, 2012; Stieglmeier *et al.*, 2014, Qin *et al.*, 2017). Both emissions of NO and the capacity to consume external NO have been observed in AOA cultures, consistent with NO being an intermediate during ammonia oxidation (Martens-Habbena *et al.*, 2015; Kozlowski *et al.*, 2016a).

NO turnover and N_2O production are therefore tightly connected to oxidation of NH_3 to NO_2^- in both AOA and AOB, since electrons used during respiration are delivered by the oxidation

of hydroxylamine. As a consequence, AOB cannot sustain nitrifier denitrification under complete anoxia, as confirmed by Anderson *et al.* (1993) for *N. europaea*, but this is apparently contradicted by Kozłowski *et al.* (2016a; 2016b), who invariably observed sharp increases in NO and N₂O production after fast O₂ depletion in micro-respirometry experiments with high cell densities.

To determine the effect of O₂ availability on NO turnover and N₂O production by AOB and AOA over longer time scales and at lower cell densities, a robotised incubation system (Molstad *et al.*, 2007) was used. Batch cultures (AOB: *N. europaea*, AOA: *N. maritimus*) with low initial cell concentrations were monitored over periods of 4 - 10 days as they gradually became limited by either O₂ or NH₃. The experiments were designed to determine the affinities for O₂ and ammonium, the product stoichiometry as controlled by the concentration of O₂, and to test specific hypotheses regarding the contrasts between AOA and AOB described above. N₂O yield in AOB was predicted to increase strongly with decreasing O₂ concentration, but not in AOA. Furthermore, it was hypothesised that cell-specific rates of N₂O production by both AOB and AOA decrease to zero in response to complete depletion of O₂ and that AOA are unable to scavenge NO in the absence of O₂. The nitrifier denitrification rate in AOB was hypothesised to be controlled by competition for electrons between terminal oxidases and nitrite and nitric oxide reductases, which was tested by comparing observed and modelled cell-specific electron flow to nitrifier denitrification as a function of O₂ concentration.

Results

Kinetics of ammonia oxidation, oxygen consumption and NO and N₂O production

Concentrations of NO₂⁻, O₂, NO, N₂O and N₂ were determined during batch growth of *N. maritimus* and *N. europaea* as either O₂ or total ammonia nitrogen (TAN, NH₄⁺ + NH₃) was depleted, depending on their initial concentrations (Fig. 1). In vials with 4 mM TAN (*N. europaea* only; Fig. 1A, D, G and J), TAN was in excess for all initial O₂ concentrations,

resulting in depletion of O₂ and NO₂⁻ production in proportion to cumulative O₂ consumption. In contrast, cultures containing medium with 1 mM TAN depleted either O₂ (vials initially with ~5 and 7 % O₂), TAN (0.5 and 1 % O₂) or both (3 % O₂).

In the vials with 7% O₂, O₂ consumption increased exponentially during the first 3 and 6 days of incubation of *N. europaea* and *N. maritimus*, respectively, until limited by declining concentrations of TAN. O₂ concentrations continued to decline after TAN depletion, but this was due to sampling dilution only (Supporting Information Fig. S4). These data were used to estimate specific growth rate (μ), cell-specific O₂ consumption rate (V_{O_2}) and growth yield (Y) during assumed unrestricted, exponential growth (Supporting Information Table S1). V_{O_2} values for *N. europaea* were similar at 1 and 4 mM TAN at ~7 fmol O₂ cell⁻¹ h⁻¹. Estimated μ and Y for the 1 mM TAN treatment were ~0.04 h⁻¹ and ~9.5 x 10¹² cells mol⁻¹ NO₂⁻, respectively, but both were ~23% lower for the 4 mM TAN treatment. This suggests some inhibition of *N. europaea* by NH₄⁺/NH₃ at the higher TAN concentration. *N. maritimus* specific growth rate was of the same order as that of *N. europaea* and V_{O_2} and Y were one order of magnitude lower and higher, respectively (Supporting Information Table S1). The initial cell densities were 0.5*10⁶ and 1*10⁶ cells mL⁻¹ for *N. europaea* and *N. maritimus*, respectively. Final cell densities in the vials with 5 and 7% O₂ were 10⁷ mL⁻¹ for *N. europaea* (1 mM TAN) and 5.5*10⁷ mL⁻¹ for *N. maritimus*.

Nitrite and cell density were measured less frequently than gas concentrations, but based on the validated relationship between cumulative O₂ consumption, NO₂⁻ accumulation and cell density, O₂ measurements were used to estimate both NO₂⁻ concentration and cell density at each gas sampling point and the rates between each gas sampling. Thus, measured rates (TAN oxidation or gas production/consumption) could be converted to cell-specific rates. The cell-specific O₂ consumption rates were used to estimate apparent maximum rates (V_{max}) and half-saturation concentrations for O₂ (k_{mO_2}) and TAN (k_{mTAN}) according to two-substrate kinetics (Table 1 and Fig. 2). Further validation of the double Michaelis-Menten model is shown by regression of model predictions against measurements (Supporting Information

Fig. S5). k_{mO_2} was similar for *N. europaea* and *N. maritimus* incubated with 1 mM NH_4^+ (2.35 and 2.13 μ M, respectively). The estimated k_{mO_2} for *N. europaea* would be 3.2 μ M, if molecular diffusion towards the cell surface was ignored. This was inconsequential for *N. maritimus*. k_{mTAN} was \sim 0.2 mM for *N. maritimus* and \sim 3 times higher for *N. europaea* (Table 1). The high V_{max} value estimated for *N. europaea* at 1 mM TAN (16.1 fmol O_2 cell $^{-1}$ h $^{-1}$) could not be realised in this experiment, since the initial TAN concentration was only \sim 2 x k_{mTAN} . At 4 mM TAN (\sim 7 x k_{mTAN}), however, O_2 consumption rates close to V_{max} would be expected. Instead, O_2 consumption rates and growth rates were lower at 4 than at 1 mM TAN and V_{max} estimated using the 4 mM TAN data was only 7.3 fmol O_2 cell $^{-1}$ h $^{-1}$ (Supporting Information Fig. S8), presumably due to partial inhibition by NH_4^+/NH_3 at 4 mM TAN as suggested above.

NO turnover

Production of NO by *N. europaea* was detectable from the beginning of the incubation, with higher rates in the treatments with low initial O_2 concentrations (Figs. 1G and H). Accumulation of NO in *N. maritimus* cultures was delayed and not detected before cultures had accumulated \sim 5 μ mol NO_2^- vial $^{-1}$ (\sim 0.1 mM NO_2^- ; Figs. 1F and I). Thus, NO production by *N. europaea* was clearly enhanced by O_2 limitation, while this was not the case for *N. maritimus* (Fig. 3). In response to O_2 depletion, *N. europaea* was able to reduce the NO concentration in some treatments (vials with 1 mM TAN and 0.5 and 1 % O_2 , Fig 1G and H). In contrast, *N. maritimus* was clearly unable to consume NO once O_2 was depleted. In response to TAN depletion (vials with initial concentrations of 5 and 7% O_2), both strains depleted NO rapidly. *N. europaea* grown at 4 mM TAN produced one order of magnitude more NO than at 1 mM. The contrasting NO kinetics of *N. maritimus* versus *N. europaea* resembles that observed by Kozlowski *et al.* (2016a) for the contrast between *N. viennensis* (AOA) and *N. multiformis* (AOB); the AOB organism increased its NO production gradually with declining oxygen concentration, while the AOA did not. However, in response to

complete oxygen depletion, Kozłowski *et al.* (2016) observed a sharp increase in NO for AOA, while this was clearly not the case for our strain.

The ability to consume NO in response to TAN depletion is better illustrated by cell-specific NO production rates after accounting for sampling dilution and NO autoxidation (Figs. 3A and B). The cell-specific NO production rate was more than one order of magnitude higher in *N. europaea* than in *N. maritimus* and the two strains responded somewhat differently to O₂ and TAN depletion. Production of NO by *N. europaea* increased with decreasing O₂ concentration, reaching a maximum at O₂ concentrations around k_{mO_2} (~2 μM). At very low O₂ concentration (<1 μM), there was net consumption (reduction) of NO in *N. europaea*, but this ceased when O₂ concentration approached zero (insert in Fig. 3A). These phenomena were not observed in *N. maritimus*, whose NO production appeared to peak at high cell densities, rather than being dependent on O₂. Both strains were able to reduce NO in response to TAN depletion as also observed for *N. maritimus* by Martens Habenna *et al.* (2015).

N₂O production kinetics and yield

Accumulation of N₂O was detectable immediately after incubation initiation of all cultures and production ceased as ammonia oxidation rate decreased, due to O₂ and/or TAN limitation (Figs. 2J, K and L). N₂O remained in the headspace in all cultures until the end of the incubation, and N₂ production was not detected. The apparent reduction of N₂O after TAN depletion was due to losses from sampling (dilution of the headspace by helium replacing sampled gas). In contrast, N₂O concentration remained almost constant after O₂ depletion. This reflects low but continued N₂O production, probably driven by minor inputs of O₂ at each sampling (~40 nmol per sampling).

The cell-specific rate of N₂O production in both strains increased with decreasing O₂ concentration, reaching maximum values at O₂ concentrations around the apparent k_{mO_2} , and rapidly declined towards zero at lower O₂ (Figs. 3C and D). The two strains reacted

differently to TAN depletion: while N₂O production by *N. europaea* declined with declining TAN concentration (vials with 3, 5 and 7% O₂), N₂O production by *N. maritimus* appeared unaffected by TAN concentration until this approached k_{mTAN} (~0.2 mM). This contrast between the two strains is better illustrated in Fig. 4, showing the relation between specific N₂O production rate (V_{N_2O}) and V_{O_2} . In *N. maritimus*, V_{N_2O} was almost proportional to V_{O_2} for all treatments within the V_{O_2} range 0 - 0.6 fmol O₂ cell⁻¹ h⁻¹. It should be noted that O₂ consumption rate in the 5 and 7% O₂ treatments became limited by TAN rather than O₂, while the opposite was the case for the 0.5 and 1% O₂ treatments. Thus, N₂O production in *N. maritimus* declined in proportion to the rate of nitrification, independent of the limiting factor (O₂ or TAN). This was not the case for *N. europaea*, where trajectories were widely different for the different O₂ treatments, with higher V_{N_2O} at lower O₂ tension.

N₂O yield (Y_{N_2O}) was estimated for each time increment. Y_{N_2O} increased as O₂ concentration approached zero for both *N. europaea* and *N. maritimus* (Fig. 5), although the levels were widely different (*N. maritimus* < *N. europaea* 1 mM TAN < *N. europaea* 4 mM TAN). As noted above, Y_{N_2O} for *N. europaea* fell towards zero as TAN was depleted (3, 5 and 7% O₂ treatments, Fig. 5A), while this was not the case for *N. maritimus* (Fig. 5C).

Electron flow to nitrifier denitrification

NO and N₂O production in *N. europaea* were modelled based on the assumption that they are controlled by the competition for electrons between terminal oxidases and denitrification enzymes, as controlled by O₂ concentration. Since measured N₂O could be derived from both nitrifier denitrification and incomplete oxidation of hydroxylamine, the latter was included in the model along with nitrifier denitrification and the total rate of N₂O and NO production (measured) was converted to electron flow (2 electrons per N₂O-N, 1 electron per NO), to be compared with model predictions. A simplified model was obtained by assuming identical affinity for cytochrome oxidase ($k_{mD} = k_{mTO}$, see Experimental procedures Eqs. 5 and 6); hence the two pathways only compete for electrons by having different V_{max} . Fig. 6

compares electron flow to nitrifier denitrification (V_{eD}) based on measurements and predictions of the fitted model ($r^2 = 0.48$; Supporting Information Fig. S6). The model captured the declining V_{eD} with declining TAN (treatments with 5 and 7% O_2) and increasing V_{eD} with declining O_2 concentration, but failed to capture the declining V_{eD} with declining O_2 concentration within the very low range (inserted panel in Fig. 6). Further, the model predicted 2- to 3-fold lower V_{eD} than that measured in the 4 mM TAN experiment (Supporting Information Fig. S10).

The alternative model, assuming that terminal oxidases (TO) and denitrification enzymes (D) have different affinities for cytochrome C_{552} , was tested by simulating steady state concentrations of reduced cytochrome C_{552} (C_{552}^*) (Supporting information Fig. S8). This gave a similar response to that shown, assuming maximum electron flow to denitrification enzymes (V_{maxeD}) and to terminal oxidases (V_{maxeTO}) to be 3 and 20 $\text{fmol e}^- \text{cell}^{-1} \text{h}^{-1}$, respectively, and $k_{mD} = 70 \cdot k_{TO}$, i.e. that TO has a stronger affinity than D (for C_{552}^*) (see Experimental procedures Eqs. 5 and 6). The discrepancy between model and measurement for the O_2 concentration range 0 - 4 μM (inserted panel in Fig. 6) could be eliminated by reducing k_{mO_2} to 0.4 μM and increasing V_{maxeD} by a factor of 4, which is effectively assuming expression of high affinity terminal oxidases and more denitrification enzymes in response to low O_2 concentrations.

It is worth noticing that the estimated V_{eD} (as measured) was very low compared to the total electron flow ($V_{eD} + V_{TO}$); the percentage of electrons directed to denitrification was $\sim 0.3\%$ for $[O_2]_s \geq 50 \mu\text{M}$, increasing gradually with declining O_2 concentrations to reach a maximum of $\sim 1.2\%$ at $[O_2]_s = 4 \mu\text{M}$ (Supporting Information Fig S7).

Discussion

Use of a robotised incubation system enabled monitoring of O_2 , NO , and N_2O kinetics by frequent sampling of headspace gas of parallel batch cultures of model archaeal and bacterial ammonia oxidisers as they grew and gradually depleted O_2 and/or TAN. This

enabled determination of kinetic parameters for O₂ consumption as a function of concentrations of O₂ and TAN, assuming a simple dual-substrate Michaelis-Menten function (see Experimental Procedures Eq. 4). With one exception, the half-saturation constants were in reasonable agreement with values found by others: a $k_{mO_2} \sim 2 \mu\text{M O}_2$ for *N. maritimus* is comparable with $3.9 \mu\text{M O}_2$ determined by Martens-Habbena *et al.* (2009), and in the lower the range of $1 - 15 \mu\text{M O}_2$ determined for *N. europaea* (Loveless and Painter, 1968) and *N. europaea*-NOB-mixed cultures (Laanbroek and Gerards, 1993; Laanbroek *et al.*, 1994). Similarly, $k_{mTAN} = 0.57 \text{ mM TAN}$ for *N. europaea* is in the lower range of previously determined values ($0.55 - 3.56 \text{ mM TAN}$; Laanbroek and Gerards, 1993; Laanbroek *et al.*, 1994; Martens-Habbena *et al.*, 2009). However, the k_{mTAN} value of 0.21 mM TAN for *N. maritimus* is three orders of magnitude higher than that determined by Martens-Habbena *et al.* (2009). This major difference is not easy to explain. The strain, growth medium and incubation temperature ($30 \text{ }^\circ\text{C}$) were the same and generated near-identical estimated maximum specific growth rates (0.027 versus 0.028 h^{-1}) in batch culture and comparable half-saturation constants for O₂ (2.2 versus $3.9 \mu\text{M O}_2$). However, Martens-Habbena *et al.* (2009) estimated k_{mTAN} by measurement of NH₄⁺ uptake rates and O₂ consumption rates following addition of NH₄⁺ to suspensions of starving cells at high cell density. Their k_{mTAN} values therefore reflected the influence of TAN concentration on specific cell activity rather than on specific growth rate in our study. Their cultures, unlike ours, were not stirred, which may have influenced diffusion of oxygen or ammonia, particularly at high cell densities, and their O₂ concentrations were higher ($150 - 170 \mu\text{M O}_2$) than in our experiments, in which the cells depleted TAN at O₂ concentrations of ~ 20 and $40 \mu\text{M O}_2$ (in the 5 and 7% initial O₂ treatments, Fig. 3), but this is unlikely to explain the high k_{mTAN} in our experiment. The ability of our strain to grow with agitation at similar maximum specific growth rate to the static cultures of Martens-Habbena *et al.* (2009) suggests some evolution or 'domestication' of the strain during repeated subculturing. This raises the possibility that the strain may also have adapted in other ways to continued laboratory since its use in the study by Martens-Habbena *et al.* (2009). The explanation for these contrasting results is crucial, since our data could be

taken to challenge the accepted view that all AOA have significantly higher affinity for TAN than AOB.

The O_2 consumption rate of *N. europaea* grown at 4 mM NH_4^+ was much lower than that predicted by the V_{max} of 17.6 fmol O_2 cell⁻¹ h⁻¹ and k_{mTAN} of 0.57 mM TAN determined in the 1 mM TAN experiment. In theory, this discrepancy could be due to substrate inhibition of ammonia monooxygenase or anabolic processes (carbon dioxide fixation, protein synthesis). However, previously estimated inhibition constants (k_i) of ammonia oxidation determined from wastewater sludges were 290 – 1,600 μ M free NH_3 (Park and Bae, 2009) were several orders of magnitude higher than our highest concentration of 4 mM TAN (equivalent to ~0.14 μ M free NH_3). A more plausible explanation is that the capacity of ammonia monooxygenase exceeds that of the anabolic processes (or hydroxylamine dehydrogenase) at high concentrations of TAN (Supporting Information Fig. S9). If so, the cells would potentially accumulate hydroxylamine at high TAN, albeit within limits imposed by hydroxylamine toxicity. Interestingly, Schmidt *et al.* (2004) reported accumulation of hydroxylamine by *N. europaea* up to steady state concentrations of 0.8 M (cytoplasm + periplasm) when provided with 2 mM NH_4^+ , although hydroxylamine appeared to be bound to proteins and could only be detected after SDS extraction. Hydroxylamine kinetics deserve further study given their potential importance as an electron donor when cells are exposed to sudden anoxia (discussed below), as well as for the apparent lag in metabolic activity in response to NH_4^+ additions to starved AOB (Chandran and Smets, 2008). Interestingly, the apparent excess capacity for ammonium oxidation would necessitate down-regulation of the expression of *amo* genes or activity of AMO in response to high ammonium concentration. In addition, the electron shunt from c_{554} to terminal oxidases and/or denitrification enzymes (Fig 7, red arrow) could be a necessary dissipation of electrons (suggested by Stein *et al.*, 2013) to stabilise the redox status of the cells during upshifts in ammonium concentration.

Many studies have demonstrated increased N_2O production by *N. europaea* and other AOB in response to O_2 limitation (reviewed by Colliver and Stephenson, 2000; Arp and Stein

2003), recently demonstrated to depend on the presence of genes coding for nitric oxide reductase (Kozłowski *et al.*, 2016b). The phenomenon is commonly ascribed to 'nitrifier denitrification', i.e. that an increasing fraction of the electrons is passed to nitrite and nitric oxide reductase as the activity of terminal oxidases become limited by low O₂ concentration (Fig. 7). Nitrifier denitrification is thought to be a significant source of N₂O emission from soils, based on indirect evidence provided by the dual isotope signature (¹⁵N, ¹⁸O) of N₂O (Kool *et al.*, 2011; Zhu *et al.*, 2013). The dual isotope method probably overestimates nitrifier denitrification, however, since it is based on the erroneous assumption that the nitrite produced by ammonium oxidation can only be denitrified by ammonia oxidizing bacteria, not by heterotrophic denitrifiers (Kool *et al.*, 2011). Our ambition was to shed some light on the denitrification capacity of AOB by stringent monitoring of O₂, NO and N₂O while the cultures were allowed to deplete either O₂ or TAN. As expected, V_{NO} and V_{N_2O} increased with decreasing O₂ concentration, reaching maximal values at O₂ concentrations around k_{mO_2} (Figs. 2A and C, Table 1). As O₂ concentration decreased further, V_{N_2O} declined towards zero, while V_{NO} reached negative values (net reduction) within the concentration range 0 - 1 μM O₂, but returned to zero as O₂ was completely depleted. Net reduction of NO is consistent with NO as an intermediate in nitrifier denitrification, and the absence of NO reduction once O₂ is depleted is consistent with the view that ammonia oxidation is the only source of electrons to drive nitrifier denitrification. V_{N_2O} and V_{NO} decreased with depletion of TAN (treatments with initial 3, 5 and 7 vol% O₂ in headspace, Fig. 3A and C). In treatments with initial 3, 5 and 7 vol% O₂, V_{O_2} decreases primarily due to TAN depletion, while in the other treatments, the decrease is primarily due to O₂ depletion. The latter treatments sustain considerably higher V_{N_2O} at intermediate V_{O_2} , but all treatments decrease to zero as V_{O_2} approach zero. This is further illustrated Fig. 5, where N₂O yield is reduced in response to depletion of TAN, and increase in response to O₂ depletion.

To extend this study beyond empirical observations of the kinetics, NO- and N₂O-production were modelled as the sum of two processes: 1) incomplete oxidation of hydroxylamine

(resulting in a constant fraction of oxidised ammonium released as NO and N₂O) and 2) NO- and N₂O-production via nitrifier denitrification, which depends on competition for electrons between TO and D (Fig. 7). The simplified model, which assumed that the terminal oxidases (TO) and denitrification enzymes (D) have identical affinities for cytochrome C₅₅₂, was indeed able to capture some of the variation in V_{eD} in the different treatments (Fig. 6) and the parameters illustrate the overwhelming competitive strength of terminal oxidases compared to denitrification: $V_{maxeTO} = 640 * V_{maxeD}$. Arguably, the reason for the preferential V_{eTO} (versus V_{eD}) could also be different affinities for cytochrome C₅₅₂ (TO stronger than D). Exploration of this with a more elaborate model, which assumed different affinities of TO and D for C₅₅₂ and assumption of $V_{maxeTO} = 6 * V_{maxeD}$, and $k_{mD} = 70 * k_{TO}$, gave a reasonable fit (Supporting Information Fig S8).

The two modelling approaches are gross simplifications of the control of electron flow, but further elaborations of branched electron flow regulation (see Otten *et al.*, 1999) were considered meaningless in the absence of direct observations to support such efforts. Nevertheless, modelling provided hypothetical explanations for the marginal denitrification capacity of *N. europaea*: it could either be due to a much lower pool of D than TO, or that the two enzyme systems have widely different affinities for cytochrome oxidases ($k_{mTO} \ll k_{mD}$). Regardless of the mechanism, the empirical data strongly suggest that a marginal fraction of the electron flow is directed to D in *N. europaea*, which underscores speculation by Arp and Stein (2003) that the primary role of the denitrification enzymes is not to sustain respiratory metabolism in response to O₂ depletion.

An interesting aspect of the modelling is the discrepancy for O₂ concentrations <4 μM: while the model predicted increasing V_{eD} with decreasing O₂ concentrations, the data showed the opposite trend (inserted panel Fig. 6.). The discrepancy could reflect a regulatory response to O₂ depletion. Plausible responses to O₂ depletion would be expression of high affinity TO and increased expression of denitrification enzymes, as observed by Beyer *et al.* (2009). To explore this, the model response to lowering the k_{TO} and increasing V_{maxeD} (See

Experimental procedures Eqs. 5 and 6) was tested. This showed that the observed increasing V_{eD} with increasing O_2 concentration (in the range 0 - 4 μM) could be obtained by combining an increase in V_{maxeD} by a factor of 4 and a reduction of k_{mO_2} from 6 to 0.4 μM O_2 (Supporting information Fig. S7). We acknowledge that the known genetic repertoire for TO in *N. europaea* is limited (Chain *et al.*, 2003), possibly lacking genes for high affinity TO.

As mentioned earlier, the electron shunt from HAO to terminal oxidases and/or D (Fig. 7) could be a mechanism of importance for redox balancing at high ammonium concentration, since the cells' capacity to oxidise ammonium at high concentrations apparently exceeds their catabolic capacity. Interestingly, this could explain the high N_2O yield at 4 mM (Fig. 3). A failure of our model to capture this phenomenon could be the gross simplifications made, for instance by assuming a single pool of cytochrome C_{552} .

Our results demonstrate that *N. europaea* has a rather modest capacity to denitrify and rates decrease to zero as O_2 is depleted, as hypothesised. This is somewhat different from the results of Kozłowski *et al.* (2016a; 2016b), who observed substantial N_2O production after complete depletion of O_2 . However, their experimental approach was very different, involving concentrated cell suspensions ($\sim 10^9$ cells mL^{-1}) enclosed in micro-respirometry chambers without headspace, leading to depletion of O_2 from 250 to 0 μM within 5 - 15 minutes. In cultures provided with NH_4^+ , they observed high N_2O production rates as O_2 reached undetectable levels (net NO accumulation was marginal compared to N_2O), but the rates decreased gradually throughout the anoxic phase of the experiments, which lasted only 20 - 30 minutes. Their observed initial N_2O production rate for *N. europaea*, immediately after O_2 depletion, was $\sim 0.5 \mu M \text{ min}^{-1}$, which is equivalent to 30 $\text{amol } N_2O \text{ cell}^{-1} \text{ h}^{-1}$ (assuming 10^9 cells mL^{-1} , as reported). In terms of electron flow to denitrification (assuming that all N_2O is produced by denitrification), this is equivalent to an electron flow rate of 120 $\text{amol cell}^{-1} \text{ h}^{-1}$, which is remarkably similar to the maximum rates observed at low O_2 concentrations in our experiments (90 - 95 $\text{amol cell}^{-1} \text{ h}^{-1}$; Fig. 6). N_2O production rates in two other AOB (*Nitrosomonas sp is79A3* and *Nitrosomonas urea*) were initially 10 - 15 times higher, but

were only sustained for minutes, decreasing gradually to $\sim 0.5 \mu\text{M min}^{-1}$ within 5 - 10 minutes (equivalent to the initial rates for *N. europaea*). Our tentative interpretation of these micro-respirometry results is that observed N_2O production during apparent anoxia could be driven by depletion of hydroxylamine (or other sources of electrons). For a cell to sustain an anoxic electron flow rate of 100 amol h^{-1} for one hour, it would have to contain a minimum of 25 μmol hydroxylamine at the time of O_2 depletion (4 mol electrons available per mol hydroxylamine), which is equivalent to an average concentration of 25 mM in the cytoplasm + periplasm (cell volume $\sim 1 \mu\text{m}^3$). In comparison, Schmidt *et al.* (2004) claim that the steady state concentration of hydroxylamine in *N. europaea* when growing aerobically at 2 mM NH_4^+ is around 800 mM (of which 5% was soluble). Thus, fast depletion of O_2 , as experienced in short term micro-respirometry experiments, is unlikely to deplete the intracellular hydroxylamine pool, hence nitrifier denitrification under anoxic conditions observed by Kozłowski *et al.* (2016a, 2016b) was plausibly sustained by a gradual oxidation of hydroxylamine (or other alternative sources of electrons). In our experiment, O_2 depletion took hours rather than minutes (Fig. 1), which is likely to have resulted in gradual depletion of hydroxylamine (or any other alternative source of electrons) long before O_2 depletion, explaining the apparent conflict between the two studies.

Modelling of electron flow in *N. maritimus* would hardly be appropriate, since the organism is equipped with nitrite reductase, but not nitric oxide reductase, and the NO produced by nitrite reductase is hypothesised to be consumed as a co-substrate in the oxidation of hydroxylamine to NO_2^- (Kozłowski *et al.*, 2016a). The observed kinetics of NO versus nitrification rates allowed inspection of this hypothesis, which would predict a positive feedback on cell-specific nitrification rate via NO accumulation, provided that NO is a free “intermediate”. The results provide little support for such a positive feedback, however (Figs. 1,2,3), which could indicate close interaction between nitrite reductase and Cu-“P460” (the hydroxylamine oxidizing enzyme), i.e. that NO is transferred directly between the two enzymes. Another conspicuous observation is that *N. maritimus* was able to deplete NO in

response to the gradual depletion of TAN, but not when depleting oxygen (Fig 1, Fig 3B). This does not necessarily conflict with the model by Kozłowski *et al.* (2016a), but suggests that their model is incomplete regarding NO turnover in these organisms.

Concluding remarks

Our study corroborate current understanding of the metabolic pathways leading to higher N₂O production by AOB than by AOA. The novelty lies in the provision of a candid assessments of their possible contribution to N₂O emissions through high resolution gas kinetics and product stoichiometry measured under physiologically realistic and ecologically relevant conditions; low cell density and gradual depletion of oxygen. The data also shed new light on the physiological role of the denitrification pathway in AOB; indicating that it plays a negligible role in sustaining their respiratory metabolism; accounting for less than 1.2% of the electron flow even under severe oxygen limitation. A more plausible physiological role for denitrification is redox balancing, which would explain the high N₂O production rates at 4 mM TAN than at 1 mM. An important environmental implication is that the N₂O yield of AOB increases with increasing ammonium concentration, and that fertilizer application level controls the N₂O/NO₂⁻ product ratio of nitrification in agricultural soils.

Experimental procedures

Culture strains and medium preparation

The AOB *Nitrosomonas europaea* ATCC 19718 was cultivated in mineral salts medium (Skinner and Walker, 1961) containing 1 mM or 4 mM (NH₄)₂SO₄ (equivalent to 50 and 200 μmol TAN vial⁻¹, respectively), phenol red (0.5 mg l⁻¹) as an indicator of pH and in addition 10

mM HEPES buffer (10 mM HEPES, 0.6 mM NaOH). pH was initially adjusted to 7.7 - 7.9 by the addition of filter-sterilised Na₂CO₃ that was also added regularly during the batch incubation to adjust the pH. The AOA *Nitrosopumilus maritimus* SCM1 was cultivated in SCM medium (Könneke *et al.*, 2005) supplemented with 1 mM NH₄Cl and buffered at pH 7.5 – 7.6 with 10 mM HEPES buffer. Both media were filter-sterilised and 50 ml medium was placed in sterile 120-ml serum bottles, each containing a magnetic stirrer flea and sealed with Teflon-coated butyl rubber septa and aluminium caps. The headspace was replaced by helium and the desired volume of pure O₂ was added aseptically as described in Molstad *et al.* (2007). Some carbonate (in equilibrium with carbon dioxide) may have been removed by gas exchange in the headspace but approximately 1 mmol and 0.5 mmol HCO₃⁻ vial⁻¹ remained in *N. europaea* and *N. maritimus* cultures, respectively. These were calculated from the initial carbon dioxide concentration in the headspace, which was 12 – 1,300 ppmv (the concentrations increased throughout incubation in proportion to the oxidation of ammonia associated with proton production leading to slight decline in pH and also ascribed to the regular addition of Na₂CO₃ (*N. europaea* only), results not shown).

Batch incubation, sampling and analysis of gas and liquid samples

Cultures with initial O₂ concentrations of 7%, 5%, 3%, 1%, 0.5% or <0.05% O₂ were prepared with 3 - 5 replicates and were inoculated with 1% (*N. europaea*) or 2% (*N. maritimus*) volumes of mid-exponential phase cultures (initial cell densities were ~0.5 x 10⁶ cells ml⁻¹ for *N. europaea* and ~10⁶ cells mL⁻¹ for *N. maritimus*). Triplicate sterile controls with an initial O₂ concentration of <0.05% were included for each experiment. Cultures were incubated in the dark at 30°C while stirring at 200 rpm to provide sufficient gas exchange between headspace and liquid. The incubations were performed in a robotised incubation system that monitors gas concentrations by taking gas samples from the headspace (Molstad *et al.*, 2007; Hassan *et al.*, 2016). In short, this was achieved by piercing the septum and pumping the gas through three sampling loops for injection to 1) a chemiluminescence detector for NO, 2) a MolSieve column for separation of N₂ and O₂

(detected by a thermal conductivity detector) and 3) a Plot column for separation of N₂O (detected both by electron-capture and thermal conductivity detectors). After sampling, the pump was reversed and the volume of gas sampled replaced with helium leading to a dilution of the headspace and a marginal leakage of O₂ and N₂ into the system, which is accounted for when calculating gas kinetics. The exact dilution and N₂ and O₂ leakage were determined by including vials filled with high concentrations of N₂ and O₂ (to determine dilution) and with pure He (to determine leakage of N₂ and O₂). These data were taken into account when calculating the rates of gas transport between headspace and liquid.

Small liquid samples (~100 µl) were taken under sterile conditions at intervals throughout the incubations for quantification of NO₂⁻ that was reduced to NO prior to the measurement in a chemiluminescence NO analyser (Roco *et al.*, 2016). Samples (~1 ml) were also taken for total cell enumeration by epifluorescence microscopy of DAPI stained cells when cultures were in mid-exponential phase as described in Lehtovirta-Morley *et al.* (2016a).

Gas kinetics calculations

As outlined in detail by Molstad *et al.* (2007), the gas concentration in the liquid during each time interval between two samplings was calculated based on the solubility of each gas (at the given temperature) and the measured transport rate (V ; mol s⁻¹), solving Eq. 2 for gas concentration in the liquid ($[G]_l$; mol l⁻¹):

$$V = k_T \cdot (k_H \cdot P_g - [G]_l) \quad (2)$$

where k_T is the transport coefficient (l s⁻¹), k_H is the solubility of the gas (mol l⁻¹ atm⁻¹) at the given temperature and P_g is the partial pressure of the gas in the headspace (average for the time increment). The transport coefficient depends on the stirring speed and, for the conditions used (30°C and 200 rpm stirring), was experimentally determined to be 0.1 l s⁻¹ (see Molstad *et al.*, 2007). The calculation of gas concentrations in the liquid by Eq. 2 proved essential for O₂, where it was found that $[O_2]_l$ was only 30 - 60% of the equilibrium

concentration ($k_H \cdot P_g$) as the cultures depleted O_2 . For NO, $[NO]_i$ reached 120 - 140% of $k_H \cdot P_{NO}$ for the time intervals with rapidly increasing concentrations, but this was essentially inconsequential for the estimated NO per vial, since the solubility of NO is very low (0.0018 mol l⁻¹ atm⁻¹ at 30°C). For N₂O, $[N_2O]_i$ reached ~108% of $k_H \cdot P_{N_2O}$ for time intervals with rapidly increasing N₂O concentrations (*N. europaea*). Thus, the calculation of liquid concentrations based on transport was essentially inconsequential for NO and N₂O, but not for O₂, which is important for determination of the affinity for O₂.

The possible consequence of transport limitation for O₂ at the cellular level was assessed, i.e. the molecular diffusion of O₂ from the bulk liquid to the cell surface. This was required because, at high rates of O₂ consumption, it cannot be taken for granted that the concentration at the cell surface is the same as that in the bulk liquid (Hassan *et al.*, 2016). Eq. 3 describes the concentration of O₂ at the cell surface ($[O_2]_s$; mol cm⁻³) of a spherical body (simplification of the rod shaped cells) with radius r (cm; $r_{N. europaea} = 6.4 \cdot 10^{-5}$ cm; $r_{N. maritimus} = 1.7 \cdot 10^{-5}$ cm), as a function of $[O_2]_i$ (mol cm⁻³), the flux towards the cell surface (J ; mol s⁻¹) and the diffusion coefficient for O₂ in water (D ; 2.2 * 10⁻⁵ cm² s⁻¹).

$$[O_2]_s = [O_2]_i - \frac{1}{4\pi r D} \quad (3)$$

The calculation was essentially inconsequential for *N. maritimus*, since $[O_2]_s$ remained >99% of $[O_2]_i$, but for *N. europaea*, which had higher rates of O₂ consumption, $[O_2]_s$ declined towards ~95 % of $[O_2]_i$ as O₂ concentration approached zero (Supporting Information Fig. S1).

Interpolations

Since cell density and NO₂⁻ were measured with lower frequency than headspace gas concentration, interpolation was required to calculate NO₂⁻ concentration and cell density for each time interval between gas samplings. Oxidised TAN and generated NO₂⁻ were determined using the cumulative O₂ consumption for individual vials. Expected O₂-

consumption:NO₂⁻-production stoichiometry is 1.5:1 (see Eq. 1), which was confirmed by measurements (Supporting Information Fig. S2). Thus, NO₂⁻ concentration for each time increment between gas samplings was estimated based on cumulated O₂ consumption. The concentration of TAN was estimated by mass balance: $TAN_t = TAN_i - N_{\text{ox}t}$, where TAN_t is the amount of TAN per vial at time t, TAN_i is the initial amount and N_{ox}t is N recovered as NO₂⁻ + NO + N₂O at time t. The measured increase in cell density was a linear function of NO₂⁻ (Supporting Information Fig. S3). Hence, for each time increment between two gas measurements, measured cumulative O₂ consumption was used to estimate cell density, NO₂⁻ and TAN concentration. These interpolations enabled modelling of electron flow towards the enzymatically produced N₂O in *N. europaea* (see below).

NO kinetics and autoxidation

NO is unstable under oxic conditions due to autoxidation, which is a “third order” reaction between O₂ and NO, proportional to O₂ concentration and the square of NO concentration (Nadeem *et al.*, 2013). As a result, apparent NO production rate (measured as an increase in concentration) may underestimate NO production and apparent NO scavenging (measured as declining NO concentration) may be falsely taken as an indication of NO scavenging by the organisms. To correct for this, NO autoxidation rate was calculated for each time increment, based on Nadeem *et al.* (2013), where NO autoxidation was measured under identical experimental condition to obtain estimates of true enzymatic net production or consumption of NO.

Kinetics

Kinetic constants for whole cell O₂ consumption were estimated on the basis of the measured rates of O₂ consumption, cell abundance and the concentrations of TAN and [O₂]_s for each time interval. Assuming that ammonia monooxygenase is the rate limiting step, two-substrate kinetics is expected, which can be described as a double Michaelis-Menten function (Splittgerber, 1983):

$$V_{O_2} = V_{max} \cdot \frac{[O_2]_s}{[O_2]_s + k_{mO_2}} \cdot \frac{[TAN]}{[TAN] + k_{mTAN}} \quad (\text{Eq. 4})$$

where V_{O_2} is the rate (fmol O_2 cell⁻¹ h⁻¹), V_{max} is the maximum rate (fmol O_2 cell⁻¹ h⁻¹), k_{mO_2} is the half-saturation constant for O_2 ($\mu\text{M } O_2$) and k_{mTAN} is the half-saturation constant for TAN ($\mu\text{M TAN}$). The parameters were estimated by non-linear regression, using the Levenberger Marquart algorithm in Minitab (Minitab Ltd, UK).

N_2O and NO production by *N. europaea* have been hypothesised to be controlled by O_2 via competition for electrons between terminal oxidases and constitutively expressed denitrification enzymes (Anderson *et al.*, 1993). This was investigated by a relatively simple modelling approach (for details see Supporting Information, “Modelling electron flow in *N. europaea* grown at 1 mM TAN” and “Modelling electron flow in *N. europaea* grown at 4 mM TAN”). The branch point was assumed to be the C_{552} , which passes electrons either to denitrification or terminal oxidases (Fig. 7). The model assumes that the flow of electrons to C_{552} (via ubiquinol and *bc1*) is determined by the rate of ammonia oxidation (which is a function of O_2 and TAN concentration) and that the electron flow to the terminal oxidases (TO) and denitrification enzymes (D) is a function of the concentrations of their respective terminal electron acceptors and the concentration of reduced C_{552} ($[C_{552}^*]$), according to Eqs. 5 and 6.

$$V_{eD} = V_{maxeD} \cdot \frac{[C_{552}^*]}{[C_{552}^*] + k_{mD}} \cdot \frac{[NO_2^-]}{[NO_2^-] + k_{mNO_2}} \quad (\text{Eq. 5})$$

$$V_{eTO} = V_{maxeTO} \cdot \frac{[C_{552}^*]}{[C_{552}^*] + k_{mTO}} \cdot \frac{[O_2]}{[O_2] + k_{mO_2}} \quad (\text{Eq. 6})$$

where V_{eD} and V_{eTO} are the rates of electron flow to denitrification enzymes and terminal oxidases, respectively, V_{maxeD} and V_{maxeTO} are their maximum rates and their affinity for C_{552}^* is given by their half-saturation constants, k_{mD} and k_{mTO} . Numerical simulation of the steady state concentration of $[C_{552}^*]$ is required unless one assumes that $k_{mNO_2} = k_{mO_2}$.

Acknowledgments

The authors are members of the Nitrous Oxide Research Alliance (NORA), a Marie Skłodowska-Curie ITN and research project under the EU's seventh framework program (FP7). GN is funded by the AXA Research Fund and CGR by a Royal Society fellowship. We thank Lars Molstad and Peter Dörsch for their generous and invaluable technical assistance. We thank Martin G Klotz for a very constructive review of our paper, and especially for pointing out the possible electron dissipation via periplasmic cytochromes, thus providing a possible explanation for the high N₂O at high ammonium concentrations.

Conflict of interests:

None declared

References

- Aakra, Å., Utåker, J.B. and Nes, I.F. (2001) Comparative phylogeny of the ammonia monooxygenase subunit A and 16S rRNA genes of ammonia-oxidizing bacteria. *FEMS Microbiol. Lett.* 205:237-242.
- Anderson, I.C., Poth, M., Homstead, J. and Burdige, D. (1993) A comparison of NO and N₂O production by the autotrophic nitrifier *Nitrosomonas europaea* and the heterotrophic nitrifier *Alcaligenes faecalis*. *Appl. Environ. Microbiol.* 59:3525-3533.
- Arp, D. J. and Stein, L.Y. (2003) Metabolism of inorganic N compounds by ammonia-oxidizing bacteria. *Crit. Rev. Biochem. Mol. Biol.* 38:471-495.
- Beyer, S., Gilch, S., Meyer, O. and Schmidt, I. (2008) Transcription of genes coding for metabolic key functions in *Nitrosomonas europaea* during aerobic and anaerobic growth. *J. Mol. Microbiol. Biotechnol.* 16:187-197.
- Bock, E. and Wagner, M. (2006) Oxidation of inorganic nitrogen compounds as an energy source. In *The Prokaryotes*. Dworkin, M., Falkow, S., Rosenberg, E., Schleifer, K.-H. and Stackebrandt, E. (eds.). New York: Springer, pp. 457-495.
- Campbell, M.A., Chain, P.S., Dang, H., El Sheikh, A.F., Norton, J.M., Ward, N. L. *et al.* (2011) *Nitrosococcus watsonii* sp. nov., a new species of marine obligate ammonia-oxidizing bacteria that is not omnipresent in the world's oceans: calls to validate the names 'Nitrosococcus halophilus' and 'Nitrosomonas mobilis'. *FEMS Microbiol. Ecol.* 76:39-48.
- Caranto, J.D., Vilbert, A.C. and Lancaster, K.M. (2016) *Nitrosomonas europaea* cytochrome P460 is a direct link between nitrification and nitrous oxide emission. *PNAS* 113:14704-14709.
- Chain, P., Lamerdin, J., Larimer, F., Regala, W., Lao, V., Land, M. *et al.* (2003) Complete genome sequence of the ammonia-oxidising bacterium and obligate chemolithoautotroph *Nitrosomonas europaea*. *J. Bacteriol.* 185:2759-2773.

Chandran, K. and Smets, B. F. (2008) Biokinetic characterization of the acceleration phase in autotrophic ammonia oxidation. *Water Environ. Res.* 80:732-739.

Colliver, B.B. and Stephenson, T. (2000) Production of nitrogen oxide and dinitrogen oxide by autotrophic nitrifiers. *Biotechnol. Adv.* 18:219-232.

Dundee, L. and Hopkins, D.W. (2001) Different sensitivities to oxygen of nitrous oxide production by *Nitrosomonas europaea* and *Nitrosolobus multiformis*. *Soil Biol. Biochem.* 33:1563-1565.

Goreau, T.J., Kaplan, W.A., Wofsy, S.C., McElroy, M.B., Valois, F.W. and Watson, S.W. (1980) Production of NO_2^- and N_2O by nitrifying bacteria at reduced concentrations of oxygen. *Appl. Environ. Microbiol.*, 40:526-532.

Hassan, J., Qu, Z., Bergaust, L. L. and Bakken, L. R. (2016) Transient accumulation of during denitrification explained by assuming cell diversification by stochastic NO_2^- and N_2O transcription of denitrification genes. *PLoS Comp. Biol.* 12:e1004621.

Hink, L., Nicol, G.W. and Prosser, J.I. (2016) Archaea produce lower yields of N_2O than bacteria during aerobic ammonia oxidation in soil. *Environ. Microbiol.* (in press).

Hooper, A.B., Maxwell, P.C. and Terry, K.R. (1978) Hydroxylamine oxidoreductase from *Nitrosomonas*: absorption spectra and content of heme and metal. *Biochem.* 17:2984-2989.

Hooper, A.B. and Terry, K.R. (1979) Hydroxylamine oxidoreductase of *Nitrosomonas*: Production of nitric oxide from hydroxylamine. *Biochim. Biophys. Acta Enzymol.* 571:12-20.

Hooper, A.B., Vanelli, T., Bergmann, D.J. and Arciero, D.M. (1997) Enzymology of the oxidation of ammonia to nitrite by bacteria. *Anton. Leeuwenhoek* 71:59-67.

Hu, H.W., Chen, D. and He, J.Z. (2015) Microbial regulation of terrestrial nitrous oxide formation: understanding the biological pathways for prediction of emission rates. *FEMS Microbiol. Rev.* 39:729-749.

Jiang, Q.Q. and Bakken, L.R. (1999) Nitrous oxide production and methane oxidation by different ammonia-oxidizing bacteria. *Appl. Environ. Microbiol.* 65:2679-2684.

Jung, M.Y., Park, S.J., Min, D., Kim, J.S., Rijpstra, W. I.C., Damsté, J.S.S. *et al.* (2011) Enrichment and characterization of an autotrophic ammonia-oxidizing archaeon of mesophilic crenarchaeal group I. 1a from an agricultural soil. *Appl. Environ. Microbiol.* 77:8635-8647.

Jung, M.Y., Well, R., Min, D., Giesemann, A., Park, S.J., Kim, J.G. *et al.* (2014) Isotopic signatures of N₂O produced by ammonia-oxidizing archaea from soils. *ISME J.* 8:1115-1125.

Kim, J.G., Jung, M.Y., Park, S.J., Rijpstra, W.I.C., Sinninghe Damsté, J.S., Madsen, E.L., *et al.* (2012) Cultivation of a highly enriched ammonia-oxidizing archaeon of thaumarchaeotal group I. 1b from an agricultural soil. *Environ. Microbiol.* 14:1528-1543.

Klotz, M.G. and Stein L.Y. (2008) Nitrifier genomics and evolution of the nitrogen cycle. *FEMS Microbiol. Lett.* 278:146-156.

Klotz, M.G. and Stein, L.Y. (2010) Genomics of ammonia-oxidizing bacteria and insights into their evolution. In *Nitrification*. Ward BB, Arp D and Klotz MG (eds). ASM Press, pp 57-93.

Könneke, M., Bernhard, A.E., José, R., Walker, C.B., Waterbury, J.B. and Stahl, D.A. (2005) Isolation of an autotrophic ammonia-oxidizing marine archaeon. *Nature* 437:543-546.

Kool D.M., van Groenigen, J.W. and Wrage, N. (2011) Source determination of nitrous oxide based on nitrogen and oxygen isotope tracing: dealing with oxygen exchange. *Meth. Enzymol.* 496:139-160.

Kozlowski, J.A., Stieglmeier, M., Schleper, C., Klotz, M.G. and Stein, L.Y. (2016a) Pathways and key intermediates required for obligate aerobic ammonia-dependent chemolithotrophy in bacteria and Thaumarchaeota. *ISME J.* 10:1836-1845.

Kozlowski, J.A., Kits, K.D. and Stein, L.Y. (2016b) Comparison of nitrogen oxide metabolism among diverse ammonia-oxidizing bacteria. *Frontiers Microbiol.* 7.

Laanbroek, H.J., Bodelier, P.L. and Gerards, S. (1994) Oxygen consumption kinetics of *Nitrosomonas europaea* and *Nitrobacter hamburgensis* grown in mixed continuous cultures at different oxygen concentrations. *Arch. Microbiol.* 161:156-162.

Laanbroek, H.J. and Gerards, S. (1993) Competition for limiting amounts of oxygen between *Nitrosomonas europaea* and *Nitrobacter winogradskyi* grown in mixed continuous cultures. *Arch. Microbiol.* 159:453-459.

Lehtovirta-Morley, L.E., Ross, J., Hink, L., Weber, E.B., Gubry-Rangin, C., Thion, C. *et al.* (2016a) Isolation of 'Candidatus Nitrosocosmicus franklandus', a novel ureolytic soil archaeal ammonia oxidiser with tolerance to high ammonia concentration. *FEMS Microbiol. Ecology* 92:fiw057.

Lehtovirta-Morley, L. E., Sayavedra-Soto, L. A., Gallois, N., Schouten, S., Stein, L. Y., Prosser, J. I., and Nicol, G. W. (2016b). Identifying Potential Mechanisms Enabling Acidophily in the Ammonia-Oxidizing Archaeon "Candidatus Nitrosotalea devanattera". *Applied and environmental microbiology*, 82(9), 2608-2619.

Löscher, C R., Kock, A., Könneke, M., LaRoche, J., Bange, H. W. and Schmitz, R.A. (2012) Production of oceanic nitrous oxide by ammonia-oxidizing archaea. *Biogeosci.* 9:2419-2429.

Loveless, J.E. and Painter, H.A. (1968) The influence of metal ion concentrations and pH value on the growth of a *Nitrosomonas* strain isolated from activated sludge. *Microbiol.* 52:1-14.

Martens-Habbena, W., Berube, P.M., Urakawa, H., José, R. and Stahl, D. A. (2009) Ammonia oxidation kinetics determine niche separation of nitrifying Archaea and Bacteria. *Nature* 461:976-979.

Martens-Habbena, W., Qin, W., Horak, R.E., Urakawa, H., Schauer, A. J., Moffett, J. W. *et al.* (2015) The production of nitric oxide by marine ammonia-oxidizing archaea and inhibition of archaeal ammonia oxidation by a nitric oxide scavenger. *Environ. Microbiol.* 17:2261-2274.

Molstad, L., Dörsch, P. and Bakken, L.R. (2007) Robotized incubation system for monitoring gases (O₂, NO, N₂O, N₂) in denitrifying cultures. *J. Microbiol. Meth.* 71:202-211.

Nadeem, S., Dörsch, P. and Bakken, L.R. (2013) Autoxidation and acetylene-accelerated oxidation of NO in a 2-phase system: Implications for the expression of denitrification in *ex situ* experiments. *Soil Biol. Biochem.* 57:606-614.

Norton, J.M., Klotz, M.G., Stein, L. Y., Arp, D.J., Bottomley, P.J., Chain, P.S., *et al.* (2008) Complete genome sequence of *Nitrosospira multiformis*, an ammonia-oxidising bacterium from the soil environment. *Appl. Environ. Microbiol.* 74:3559-3572.

Otten, M. F., Reijnders, W.N., Bedaux, J.J., Westerhoff, H.V., Krab, K. and Van Spanning, R. J. (1999) The reduction state of the Q-pool regulates the electron flux through the branched respiratory network of *Paracoccus denitrificans*. *Eur. J. Biochem.* 261:767-774.

Park S. and Bae W. (2009) Modelling the kinetics of ammonium oxidation and nitrite oxidation under simultaneous inhibition by free ammonia and free nitrous oxide. *Process Biochem.* 44:631-640.

Qin, W., Meinhardt, K.A., Moffett, J.W., Devol, A.H., Virginia Armbrust, E., Ingalls, A.E. and Stahl, D.A. (2017) Influence of oxygen availability on the activities of ammonia-oxidizing archaea. *Environ. Microbiol. Rep.* 9:250-256.

Prosser, J.I. (1990) Autotrophic nitrification in bacteria. *Adv. Microb. Physiol* 30:125-181.

Remde, A. and Conrad, R. (1990) Production of nitric oxide in *Nitrosomonas europaea* by reduction of nitrite. *Archiv. Microbiol.*, 154:187-191.

Roco, C.A., Bergaust, L.L., Shapleigh, J.P. and Yavitt, J.B. (2016) Reduction of nitrate to nitrite by microbes under oxic conditions. *Soil Biol. Biochem.* 100:1-8.

Santoro, A.E., Buchwald, C., McIlvin, M.R. and Casciotti, K.L. (2011) Isotopic signature of N₂O produced by marine ammonia-oxidizing archaea. *Sci.* 333:1282-1285.

Schmidt, I., Look, C., Bock, E. and Jetten, M.S. (2004) Ammonium and hydroxylamine uptake and accumulation in *Nitrosomonas*. Microbiol. 150:1405-1412.

Simon, J. and Klotz, M.G. (2013) Diversity and evolution of bioenergetics systems involved in microbial nitrogen compound transformations. Biochim. Biophys. Acta 1827:114-135.

Skinner, F.A. and Walker, N. (1961) Growth of *Nitrosomonas europaea* in batch and continuous culture. Arch. Mikrobiol. 38:339-349.

Spang, A., Poehlein, A., Offre, P., Zumbärgel, S., Haider, S., Rychlik, *et al.* (2012) The genome of the ammonia-oxidizing *Candidatus Nitrososphaera gargensis*: insights into metabolic versatility and environmental adaptations. Environ. Microbiol. 14:3122-3145.

Spittgerber, A.G. (1983) Simplified treatment of two-substrate enzyme kinetics. J. Chem. Educ. 60:651-655.

Stein, L.Y. (2011). Surveying N₂O-producing pathways in bacteria. Meth. Enzymol. 486:131–152.

Stieglmeier, M., Mooshammer, M., Kitzler, B., Wanek, W., Zechmeister-Boltenstern, S., Richter, A. *et al.* (2014) Aerobic nitrous oxide production through N-nitrosating hybrid formation in ammonia-oxidizing archaea. ISME J. 8:1135-1146.

Tourna, M., Stieglmeier, M., Spang, A., Könneke, M., Schintlmeister, A., Urich, T. *et al.* (2011) *Nitrososphaera viennensis*, an ammonia oxidizing archaeon from soil. PNAS 108:8420-8425.

Vajjala, N., Martens-Habbena, W., Sayavedra-Soto, L.A., Schauer, A., Bottomley, P.J., Stahl, D.A. *et al.* (2013) Hydroxylamine as an intermediate in ammonia oxidation by globally abundant marine archaea. PNAS 110:1006-1011.

Walker, C.B., De La Torre, J.R., Klotz, M.G., Urakawa, H., Pinel, N., Arp, D.J., *et al.* (2010) *Nitrosopumilus maritimus* genome reveals unique mechanisms for nitrification and autotrophy in globally distributed marine crenarchaea. PNAS 107:8818-8823.

Whittaker, M., Bergman, D., Arciero, D. and Hooper, A.B. (2000) Electron transfer during the oxidation of ammonia by the chemolithotrophic bacterium *Nitrosomonas europaea*. *Biochim. Biophys. Acta* 1459:346-355.

Wrage, N., Velthof, G. L., Van Beusichem, M.L. and Oenema, O. (2001) Role of nitrifier denitrification in the production of nitrous oxide. *Soil Biol. Biochem.* 33:1723-1732.

Yu, K. and Chandran, K. (2010) Strategies of *Nitrosomonas europaea* 19718 to counter low dissolved oxygen and high nitrite concentrations. *BMC Microbiol.* 10:70

Zhu, X., Burger, M., Doane, T. A. and Horwath, W.R. (2013) Ammonia oxidation pathways and nitrifier denitrification are significant sources of N₂O and NO under low oxygen availability. *PNAS* 110:6328-6333.

Zhu-Barker, X., Cavazos, A.R., Ostrom, N.E., Horwath, W.R. and Glass, J.B. (2015) The importance of abiotic reactions for nitrous oxide production. *Biogeochem.* 126:251-267.

Figure and Table legends

Figures

Fig. 1. Oxygen consumption kinetics (A - C), nitrite production (D - F) and nitrogen gas turnover (G - L) in 50-mL batch cultures contained in gas-tight serum bottles. Cultures of *N. europaea* (incubated with 4 mM TAN: A, D, G, J; incubated with 1 mM TAN: B, E, H, K) and *N. maritimus* (incubated with 1 mM TAN: C, F, I, L) were grown in mineral salts medium at a range of initial O₂ concentrations (see legend). O₂ was depleted entirely at low initial O₂ concentrations, while TAN rather than O₂ limited activity at high initial O₂ concentrations (A - C). NO₂⁻ concentration (D - F) is calculated on the basis of cumulative O₂ consumption and was similar to that measured (x) (Supporting Information Fig. S2). 1 nmol NO vial⁻¹ is equivalent to a concentration of 0.62 nM in the liquid. Means and standard errors of 3 - 5 replicate cultures are plotted.

Fig. 2. Oxygen- and TAN-dependent O₂ consumption rate by *N. europaea* (A, B) and *N. maritimus* (C, D) incubated with an initial TAN concentration of 1 mM. Three-dimensional plots (A, C) show cell-specific O₂ consumption rates (single time increment, individual vials) as a function of O₂ concentration at the cell surface ([O₂]_s; calculated from transport kinetics, see Experimental procedures) and the concentration of TAN. A double Michaelis-Menten equation (see Experimental procedures Eq. 4) was fitted to the data and is represented as a surface; measurements are shown as vertical lines from measurements to model values (red: measurement > model, blue: measurement < model). Two-dimensional plots (B, D) show the rates against O₂ concentrations for the 0.5 - 3% O₂ treatments at low ([O₂]_s, together with model estimates. Estimated kinetic parameters are shown in Table 1, and correlation between model estimates and measurements ($r^2 \geq 0.98$ for both strains) is shown in Supporting Information Fig. S5.

Fig. 3. Cell-specific rates of NO and N₂O production by *N. europaea* (A, C) and *N. maritimus* (B, D) incubated with an initial TAN concentration of 1 mM. The rate of NO production (V_{NO}) (A, B) is corrected for NO autoxidation and reflects enzymatic production (positive values) and consumption (negative values). Cultures depleted either O₂ and/or TAN entirely, depending on the initial O₂ concentration in the headspace (see legend). Limitation of O₂ and/or TAN also affected the rate of N₂O production (C, D).

Fig. 4. Relationship between velocity of N₂O (V_{N_2O}) production and O₂ consumption rates (V_{O_2}) of *N. europaea* (A) and *N. maritimus* (B) incubated with 1 mM TAN at a range of initial O₂ concentrations (see legend).

Fig. 5. Oxygen-dependent N₂O yield of *N. europaea* (incubated with 1 mM TAN, A, or with 4 mM TAN, B) and *N. maritimus* (incubated with 1 mM TAN, C). N₂O yield is expressed as N₂O-N per NO₂⁻-N generated from ammonia oxidation in cultures incubated with a range of initial O₂ concentrations (see legend).

Fig. 6. Electron flow to denitrification (amol e⁻ cell⁻¹ h⁻¹) for *N. europaea* growing on 1 mM TAN; model predictions versus measurements. The electron flow rate to nitrifier denitrification (V_{eD}) are based on measurements (NO and N₂O concentration) of single time increment values. Model predictions are plotted as continuous lines, using the experimentally determined concentrations of ([O₂]_s and [TAN]) as inputs (average values for replicate vials at each time point). The insert highlights the declining electron flow to nitrifier denitrification at very low ([O₂]_s concentration and the failure of the model to capture this phenomenon. The model parameters (see Supporting Information, “Modelling electron flow in *N. europaea* grown at 1 mM TAN”) are $Y_{HAO} = 0.0019$ (proportion of oxidised hydroxylamine-N released as N₂O-N), $k_{mO_2} = 11.2 \mu\text{M O}_2$ (half-saturation concentration for terminal oxidases), $V_{maxeTO} = 640 \times V_{maxeD}$ (V_{maxeTO}

and V_{maxeD} are the maximum rates of electron flow to terminal oxidases and denitrification, respectively).

Fig. 7. Simplified electron flow in *N. europaea*. The 4 electrons per NO_2^- produced by hydroxylamine dehydrogenase (HAO) are relayed to the quinone pool (Q) most plausibly via membrane cytochrome c_{m552} , or via periplasmic C_{554} and C_{m552} (see discussion by Simon and Klotz, 2013). Ammonia monooxygenase (AMO) draws 2 electrons from the quinone pool and the remaining 2 electrons are passed either to NAD (\rightarrow NADH, reducing power for CO_2 assimilation) or to periplasmic cytochrome C_{552} via the cytochrome bc1 complex. C_{552} is a branching point, delivering electrons either to terminal oxidases (TO) or to the denitrification enzymes (D), i.e. nitrite reductase and nitric oxide reductase (nirK and NorB, Arp and Stein, 2003). Several different C_{552} proteins may be involved at this branching point (Klotz and Stein, 2010). Our modelling of competition for electrons (TO versus D) assuming one common electron donor is therefore a gross simplification. Proton motive force is generated by *bc1* and TO (Klotz and Stein, 2008; Kozłowski et al., 2016a), while the electron transport from HAO to Q may be electroneutral (Simon and Klotz, 2013). An electron shunt from c_{554} to C_{552} is indicated (red dashed arrow), which has been suggested by Stein *et al.* (2013) as an electron neutral pathway to D.

Table legend.

Table 1. Estimated kinetic parameters for O_2 consumption as a function of O_2 and TAN concentration in *N. europaea* and *N. maritimus*.

Tables and Figures:

Table 1. Estimated kinetic parameters for O₂ consumption rate as a function of O₂ and TAN concentration in *N. europaea* and *N. maritimus*.

	V_{max}^{\S} (fmol O ₂ cell ⁻¹ h ⁻¹)	$k_{O_2}^{\S}$ (μM O ₂)	k_{TAN}^{\S} (mM TAN)
<i>N. europaea</i>	17.6 (0.6) [15.6-17.9]	2.35 (0.13) [2.2-2.6]	0.565 (0.04) [0.44-0.59]
<i>N. maritimus</i>	1.0 (0.01) [0.98-1.03]	2.13 (0.08) [2.0-2.3]	0.20 (0.02) [0.18-0.23]

[§] Kinetic parameters were estimated from cultures that were incubated with an initial TAN concentration of 1 mM and a range of O₂ concentrations. The dataset for each strain was fitted with Eq. 4. Standard deviations are displayed in parentheses and 95% confidence intervals in brackets.

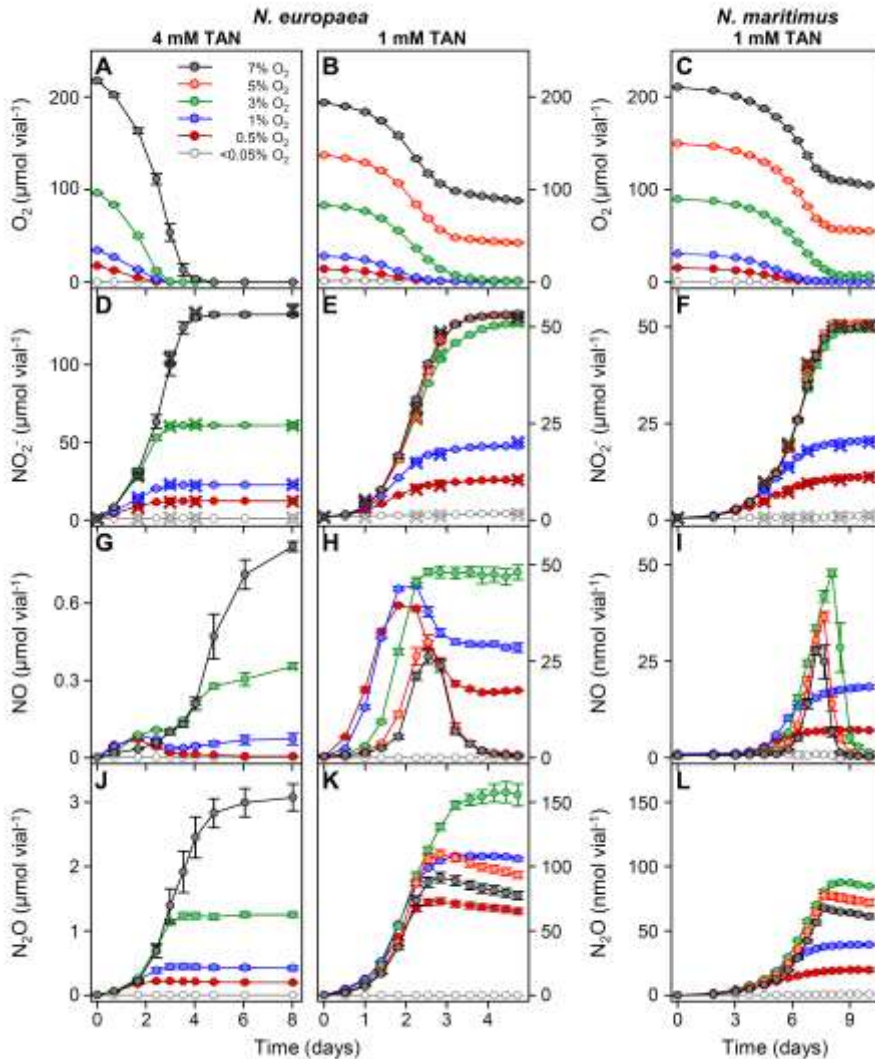
Fig. 1

Fig. 1. Oxygen consumption kinetics (A - C), nitrite production (D - F) and nitrogen gas turnover (G - L) in 50-mL batch cultures contained in gas-tight serum bottles. Cultures of *N. europaea* (incubated with 4 mM TAN: A, D, G, J; incubated with 1 mM TAN: B, E, H, K) and *N. maritimus* (incubated with 1 mM TAN: C, F, I, L) were grown in mineral salts medium at a range of initial O₂ concentrations (see legend). O₂ was depleted entirely at low initial O₂ concentrations, while TAN rather than O₂ limited activity at high initial O₂ concentrations (A - C). NO₂⁻ concentration (D - F) is calculated on the basis of cumulative O₂ consumption and was similar to that measured (x) (Supporting Information Fig. S2). 1 nmol NO vial⁻¹ is equivalent to a concentration of 0.62 nM in the liquid. Means and standard errors of 3 - 5 replicate cultures are plotted.

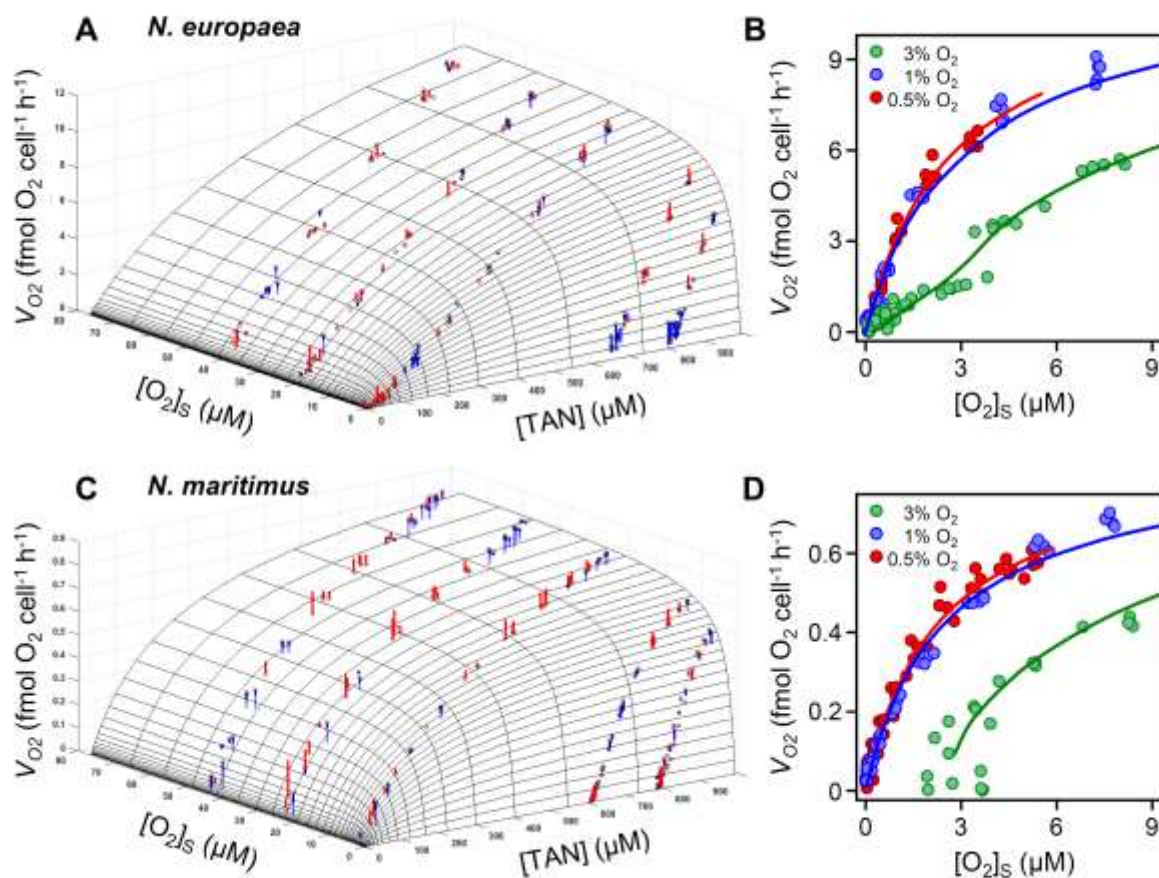
Fig. 2

Fig. 2. Oxygen- and TAN-dependent O₂ consumption rate by *N. europaea* (A, B) and *N. maritimus* (C, D) incubated with an initial TAN concentration of 1 mM. Three-dimensional plots (A, C) show cell-specific O₂ consumption rates (single time increment, individual vials) as a function of O₂ concentration at the cell surface ([O₂]_s; calculated from transport kinetics, see Experimental procedures) and the concentration of TAN. A double Michaelis-Menten equation (see Experimental procedures Eq. 4) was fitted to the data and is represented as a surface; measurements are shown as vertical lines from measurements to model values (red: measurement > model, blue: measurement < model). Two-dimensional plots (B, D) show the rates against O₂ concentrations for the 0.5 - 3% O₂ treatments at low ([O₂]_s, together with model estimates. Estimated kinetic parameters are shown in Table 1, and correlation

between model estimates and measurements ($r^2 \geq 0.98$ for both strains) is shown in Supporting Information Fig. S5.

Fig. 3

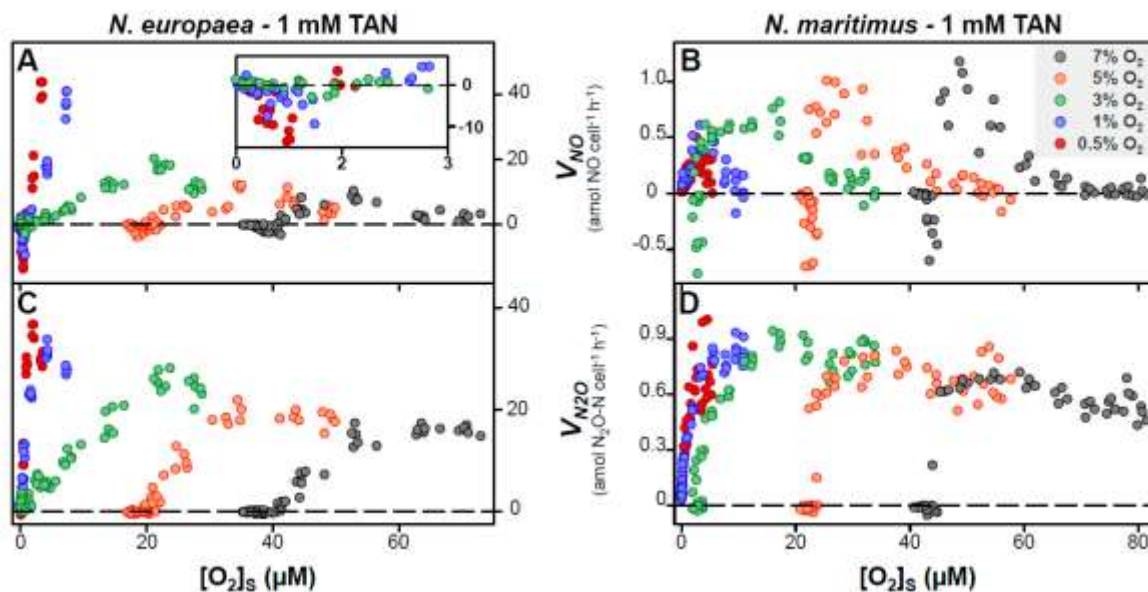


Fig. 3. Cell-specific rates of NO and N₂O production by *N. europaea* (A, C) and *N. maritimus* (B, D) incubated with an initial TAN concentration of 1 mM. The rate of NO production (V_{NO}) (A, B) is corrected for NO autoxidation and reflects enzymatic production (positive values) and consumption (negative values). Cultures depleted either O₂ and/or TAN entirely, depending on the initial O₂ concentration in the headspace (see legend). Limitation of O₂ and/or TAN also affected the rate of N₂O production (C, D).

Fig. 4

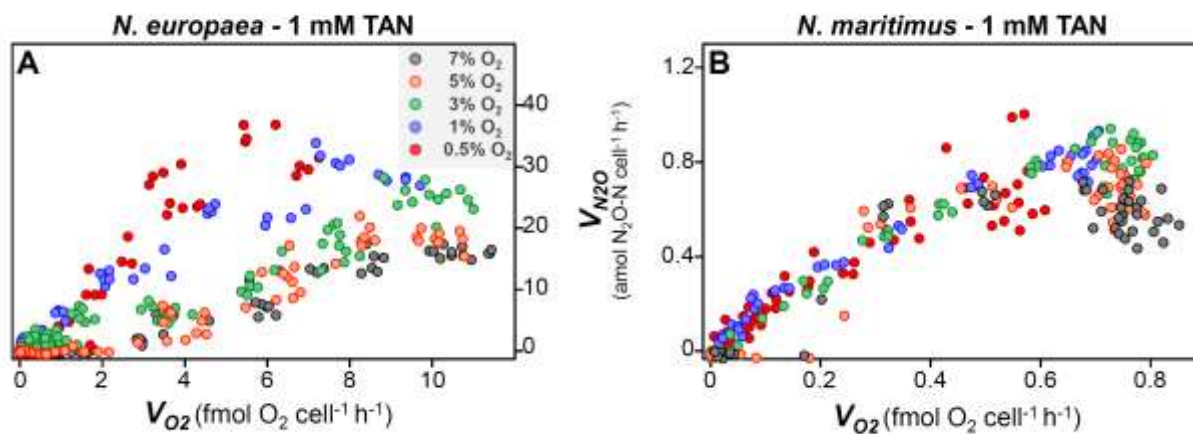


Fig. 4. Relationship between velocity of N₂O (V_{N_2O}) production and O₂ consumption rates (V_{O_2}) of *N. europaea* (A) and *N. maritimus* (B) incubated with 1 mM TAN at a range of initial O₂ concentrations (see legend).

Accepted

Fig. 5

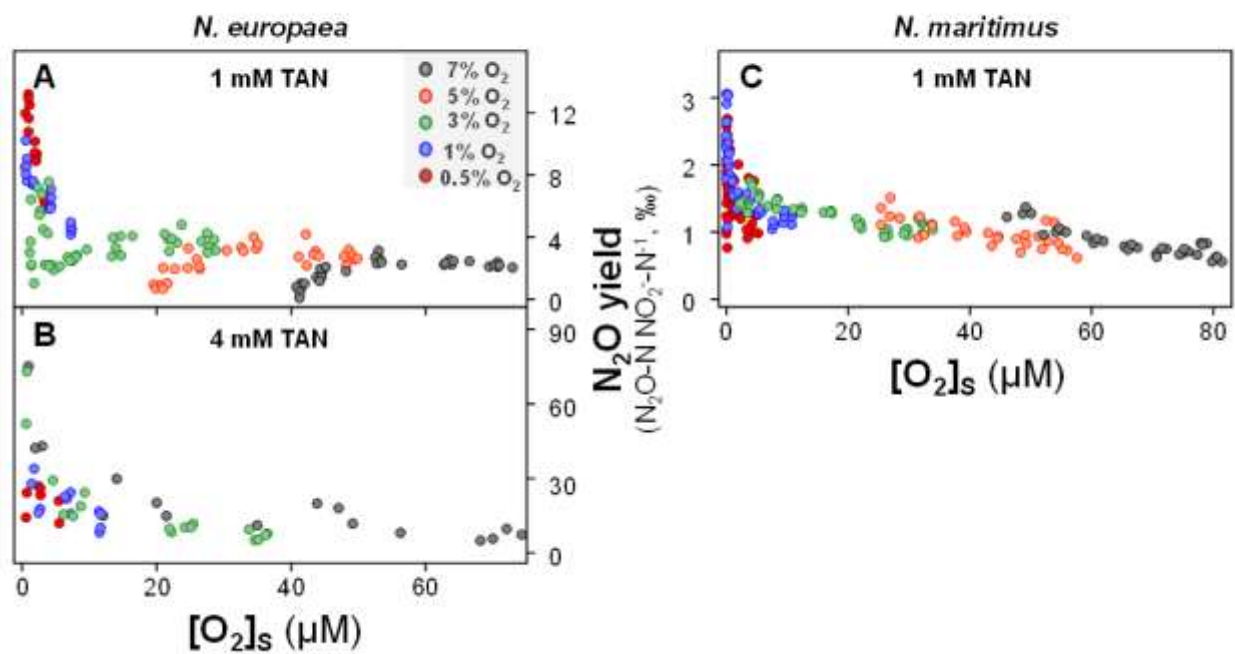


Fig. 5. Oxygen-dependent N_2O yield of *N. europaea* (incubated with 1 mM TAN, A, or with 4 mM TAN, B) and *N. maritimus* (incubated with 1 mM TAN, C). N_2O yield is expressed as N_2O-N per NO_2^-N generated from ammonia oxidation in cultures incubated with a range of initial O_2 concentrations (see legend).

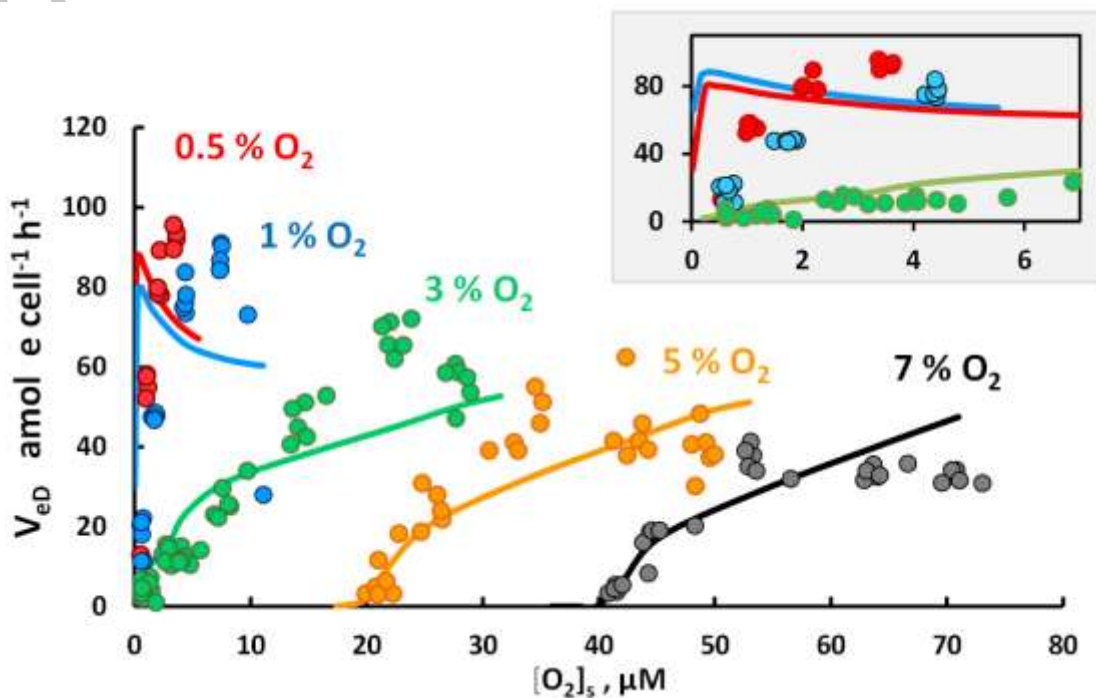


Fig. 6. Electron flow to denitrification ($\text{amol e}^- \text{cell}^{-1} \text{h}^{-1}$) for *N. europaea* growing on 1 mM TAN; model predictions versus measurements. The electron flow rate to nitrifier denitrification (V_{eD}) are based on measurements (NO and N_2O concentration) of single time increment values. Model predictions are plotted as continuous lines, using the experimentally determined concentrations of ($[\text{O}_2]_s$ and $[\text{TAN}]$) as inputs (average values for replicate vials at each time point). The insert highlights the declining electron flow to nitrifier denitrification at very low ($[\text{O}_2]_s$) concentration and the failure of the model to capture this phenomenon. The model parameters (see Supporting Information, “Modelling electron flow in *N. europaea* grown at 1 mM TAN”) are $Y_{\text{HAO}} = 0.0019$ (proportion of oxidised hydroxylamine-N released as $\text{N}_2\text{O-N}$), $k_{m\text{O}_2} = 11.2 \mu\text{M O}_2$ (half-saturation concentration for terminal oxidases), $V_{\text{maxeTO}} = 640 \times V_{\text{maxeD}}$ (V_{maxeTO} and V_{maxeD} are the maximum rates of electron flow to terminal oxidases and denitrification, respectively).

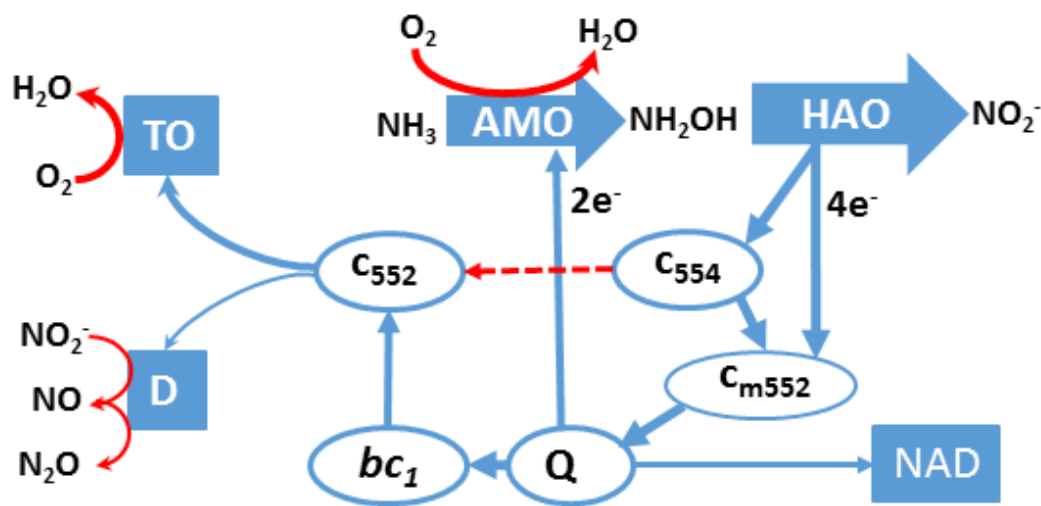


Fig. 7. Simplified electron flow in *N. europaea*. The 4 electrons per NO_2^- produced by hydroxylamine dehydrogenase (HAO) are relayed to the quinone pool (Q) most plausibly via membrane cytochrome C_{m552} , or via periplasmic C_{554} and C_{m552} (see discussion by Simon and Klotz, 2013). Ammonia monooxygenase (AMO) draws 2 electrons from the quinone pool and the remaining 2 electrons are passed either to NAD (\rightarrow NADH, reducing power for CO_2 assimilation) or to periplasmic cytochrome C_{552} via the cytochrome bc_1 complex. C_{552} is a branching point, delivering electrons either to terminal oxidases (TO) or to the denitrification enzymes (D), i.e. nitrite reductase and nitric oxide reductase (*nirK* and *NorB*, Arp and Stein, 2003). Several different C_{552} proteins may be involved at this branching point (Klotz and Stein, 2010). Our modelling of competition for electrons (TO versus D) assuming one common electron donor is therefore a gross simplification. Proton motive force is generated by bc_1 and TO (Klotz and Stein, 2008; Kozłowski et al., 2016a), while the electron transport from HAO to Q may be electroneutral (Simon and Klotz, 2013). An electron shunt from C_{554} to C_{552} is indicated (red dashed arrow), which has been suggested by Stein *et al.* (2013) as an electron neutral pathway to D.